Research Article | Vol. 26, No. 2 | 22 Jan 2018 | OPTICS EXPRESS 1305

Optics EXPRESS

Integrated InP polarization rotator using the plasmonic effect

SHINMO AN* AND O-KYUN KWON

ICT Materials & Components Research Laboratory, Electronics and Telecommunications Research Institute (ETRI), 218 Gajeong-ro, Yuseong-gu Daejeon, 34129, South Korea
*shinmo.an@etri.re.kr

Abstract: we report on an integrated InP based polarization rotator scheme using the plasmonic effect. It operates as a half-wave retarder in ridge waveguide structure. The rotation angle of the eigenmode axes of the half-wave retarder waveguide is determined by the position off a bottom corner of a metal layer placed above the waveguide core in the upper cladding region. The simple rotator structure enables an easy and tolerant fabrication process. The length of the fabricated device is less than 50 µm, and a polarization extinction ratio (PER) of 20 dB has been achieved.

© 2018 Optical Society of America under the terms of the OSA Open Access Publishing Agreement

OCIS codes: (130.3120) Integrated optics devices; (130.5440) Polarization-selective devices; (230.7370) Waveguides; (250.5403) Plasmonics.

References and links

1. K. Roberts, D. Beckett, D. Boertjes, J. Berthold, and C. Laperle, "100G and beyond with digital coherent signal processing," IEEE Commun. Mag. **48**(7), 62–69 (2010).
2. S. Michel, "Why complex modulated optical signals? " Lightwave **1**, 18 (2013).
3. T. Optical and I. Forum, Technology Options for 400G Implementation, in *Optical Networking Forum (OIF), OIF-Tech-Options-400G-01.0*. July (2015).
4. Optical Internetworking Forum, Implementation Agreement for Integrated Polarization Multiplexed Quadrature Modulated Transmitters v01.1 (2013).
5. H. El-Refaei, D. Yevick, and T. Jones, "Slanted-Rib Waveguide InGaAsP – InP Polarization Converters," J. Lightwave Technol. **22**(5), 1352–1357 (2004).
6. U. Khalique, Y. C. Zhu, J. J. G. M. van der Tol, L. M. Augustin, R. Hanfoug, F. H. Groen, P. J. van Veldhoven, M. K. Smit, M. van de Moosdijk, W. de Laat, and K. Simon, "Ultrashort Polarization Converter on InP/InGaAsP Fabricated by Optical Lithography," in *Integrated Photonics Research and Applications* (Optical Society of America, 2005), p. IWA3.
7. L. M. Augustin, J. J. G. M. van der Tol, E. J. Geluk, and M. K. Smit, "Short Polarization Converter Optimized for Active – Passive Integration in InGaAsP – InP," IEEE Photonics Technol. Lett. **19**(20), 1673–1675 (2007).
8. M. Kotlyar, L. Bolla, M. Midrio, L. O'Faolain, and T. Krauss, "Compact polarization converter in InP-based material," Opt. Express **13**(13), 5040–5045 (2005).
9. Z. Wang and D. Dai, "Ultrasmall Si-nanowire-based polarization rotator," J. Opt. Soc. Am. B **25**(5), 747–753 (2008).
10. M. Aamer, A. M. Gutierrez, A. Brimont, D. Vermeulen, G. Roelkens, J. M. Fedeli, A. Hakansson, and P. Sanchis, "CMOS compatible silicon-on-insulator polarization rotator based on symmetry breaking of the waveguide cross section," IEEE Photonics Technol. Lett. **24**(22), 2031–2034 (2012).
11. B. M. Holmes and D. C. Hutchin, "Realization of novel low-loss monolithically integrated passive waveguide mode converters," IEEE Photonics Technol. Lett. **18**(1), 43–45 (2006).
12. H. Fukuda, K. Yamada, T. Tsuchizawa, T. Watanabe, H. Shinojima, and S. Itabashi, "Polarization rotator based on silicon wire waveguides," Opt. Express **16**(4), 2628–2635 (2008).
13. C. van Dam, L. H. Spiekman, F. P. G. M. van Ham, F. H. Groen, J. J. G. M. van der Tol, I. Moerman, W. W. Pascher, M. Hamacher, H. Heidrich, C. M. Weinert, and M. K. Smit, "Novel Compact Polarization Converters Based on Ultra Short Bends," IEEE Photonics Technol. Lett. **8**(10), 1346–1348 (1996).
14. M. R. Watts and H. A. Haus, "Integrated mode-evolution-based polarization rotators," Opt. Lett. **30**(2), 138–140 (2005).
15. J. Zhang, M. Yu, G. Q. Lo, and D. L. Kwong, "Silicon-waveguide-based mode evolution polarization rotator," IEEE J. Sel. Top. Quantum Electron. **16**(1), 53–60 (2010).
16. L. Chen, C. R. Doerr, and Y.-K. Chen, "Compact polarization rotator on silicon for polarization-diversified circuits," Opt. Lett. **36**(4), 469–471 (2011).
17. L. Liu, Y. Ding, K. Yvind, and J. M. Hvam, "Silicon-on-insulator polarization splitting and rotating device for polarization diversity circuits," Opt. Express **19**(13), 12646–12651 (2011).

#308170 https://doi.org/10.1364/OE.26.001305
Journal © 2018 Received 28 Sep 2017; revised 29 Dec 2017; accepted 3 Jan 2018; published 12 Jan 2018

18. D. Dai and J. E. Bowers, "Novel concept for ultracompact polarization splitter-rotator based on silicon nanowires," Opt. Express **19**(11), 10940–10949 (2011).
19. H. Guan, A. Novack, M. Streshinsky, R. Shi, Q. Fang, A. E.-J. Lim, G.-Q. Lo, T. Baehr-Jones, and M. Hochberg, "CMOS-compatible highly efficient polarization splitter and rotator based on a double-etched directional coupler," Opt. Express **22**(3), 2489–2496 (2014).
20. J. Zhang, S. Zhu, H. Zhang, S. Chen, G. Lo, and D. Kwong, "An Ultracompact Surface Plasmon Polariton-Effect-Based Polarization Rotator," IEEE Photonics Technol. Lett. **23**(21), 1606–1608 (2011).
21. J. N. Caspers, J. S. Aitchison, and M. Mojahedi, "Experimental demonstration of an integrated hybrid plasmonic polarization rotator," Opt. Lett. **38**(20), 4054–4057 (2013).
22. J. Chee, S. Zhu, and G. Q. Lo, "CMOS compatible polarization splitter using hybrid plasmonic waveguide," Opt. Express **20**(23), 25345–25355 (2012).
23. S. Kim and M. Qi, "Polarization rotation and coupling between silicon waveguide and hybrid plasmonic waveguide," Opt. Express **23**(8), 9968–9978 (2015).
24. Z. Li, M.-H. Kim, C. Wang, Z. Han, S. Shrestha, A. C. Overvig, M. Lu, A. Stein, A. M. Agarwal, M. Lončar, and N. Yu, "Controlling propagation and coupling of waveguide modes using phase-gradient metasurfaces," Nat. Nanotechnol. **12**(7), 675–683 (2017).
25. S. An, H.-S. Lee, Y.-B. Jeong, Y. C. Jun, S. G. Lee, S.-G. Park, H. Lee, and O. Beom-Hoan, "Nanofocusing of light using three-dimensional plasmonic mode conversion," Opt. Express **21**(23), 27816–27825 (2013).
26. Z. Chen, L. Yan, W. Pan, B. Luo, Y. Guo, H. Jiang, A. Yi, Y. Sun, and X. Wu, "Transmission of multi-polarization-multiplexed signals: another freedom to explore?" Opt. Express **21**(9), 11590–11605 (2013).

1. Introduction

The ever-increasing data capacity in optical fiber communications has led to spectral efficiency being considered more important than the conventional symbol rate. A higher spectral efficiency is drawn by advanced modulation formats. It is based on phase shift keying (PSK) techniques such as quadrature phase shift keying (QPSK) and quadrature amplitude modulation (QAM). The so-called coherent optical communications has become the next-generation optical communication standard protocol [1–3]. With advanced modulation formats, polarization division multiplexing (PDM), furthermore, has been utilized in coherent communications. In PDM, two orthogonally polarized optical signals with the same frequency are transmitted over the same optical fiber (dual-polarization) as shown in Fig. 1. With dual-PDM, the spectral efficiency increases by a factor of two without sacrificing channel bandwidth. For the same frequency, the two polarization states of the light are derived from a linearly polarized light source. For the implementation of dual-PDM, a polarization rotator that rotates the polarization state of the light source to an orthogonal state, and a polarization combiner that combines two orthogonal states of the light, are needed [4]. The Integrated polarization rotator has been extensively studied using periodic slanted rib waveguides [5–7], slanted grating etching [8], partial etching [9,10], reactive ion-etch lag [11], off-axis double cores [12], waveguide bends [13], mode evolution [14–16], asymmetrical directional coupler [17–19], surface plasmon [20–23], and phase-gradient meta surface [24].

Especially, epitaxially grown ridge waveguides from materials such as InGaAsP on InP have been studied since the early 90s because of the significance, which can be integrated with active light sources or high-speed electro-optic modulators. This waveguide structure has a strong refractive index difference between the undercladding and uppercladding layers. The former is normally high-refractive-index (> 3.0) semiconductor material, and the latter is a low-refractive-index (< 2.0) dielectric material. Owing to the epitaxial grown conditions, the refractive index of the undercladding layer is similar to that of the core material rather than the dielectric uppercladding layer. This strong refractive index asymmetry in the cladding materials disturbs the rotation of the fundamental eigenmode axes, which is induced by an index asymmetry in the core, in the polarization rotator. To overc ome this material condition, previous studies necessitated steep and tight fabrication-tolerant structures.

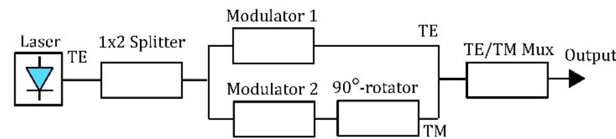

Fig. 1. Dual polarization division multiplexed transmitter.

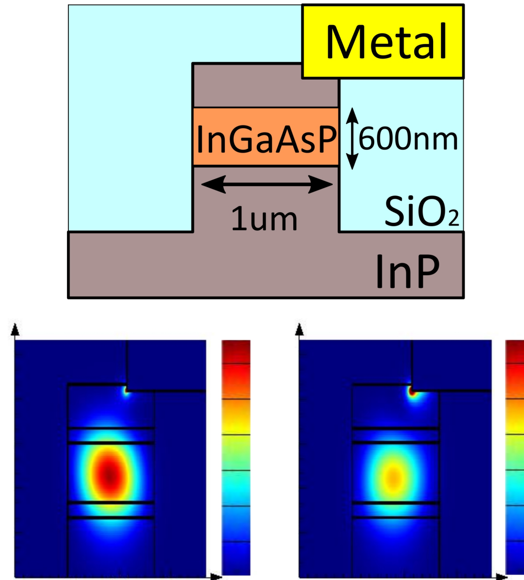

Fig. 2. InP polarization rotator. The eigenmode axes of the waveguide are rotated in the diagonal direction (45° rotation) with respect to the position of a bottom corner of the metal (Au) layer above the core. The rotated eigenmode axes in the waveguide behave as a birefringent material. The bottom insets show the electric field intensity of the rotated eigenmodes for InP ridge waveguide.

In this paper, we propose an integrated InP polarization rotation scheme using surface plasmon effect. It has a simple and fabrication tolerant rotator structure.

2. Device structure and simulation results

2.1 InP polarization rotator concept

The device consists of a core waveguide and a metal layer placed in the uppercladding layer. Figure 2 shows an InGaAsP deep-ridge-type waveguide on an InP material. One side corner of the metal layer is placed above the core. Here, the fundamental eigenmodes of the core interact with the surface plasmon mode in the metal and rotate according to the position of a bottom corner of the metal layer. The metal material can be a noble metal (Au, Ag, etc.) and can also include Al and Cu for CMOS-compatible fabrication processes. Polarization rotation due to the influence of the metal strip was reported in our previous work [25].

In this work, we apply this phenomenon to control the angle of the eigenmode axes in the waveguide. The bottom insets in Fig. 2 show the rotated eigenmode electric field intensities of the InP rotator at a wavelength of 1.55 µm. Majority of the electric field distribution is aligned in the diagonal (45°) direction. When a linearly polarized (TE–parallel and TM–longitudinal) light is incident on the rotator, the beam power is equally projected on each eigenmode axis and one of the eigenmodes undergoes a phase retardation by the effective index difference because the rotated eigenmode axes behave as a birefringent material. The

rotator is designed at a length of half-wave (π) phase retardation resulting in full polarization conversion (90° rotation).

2.2 Simulation condition

The mode profile of the polarization rotator for InP ridge waveguide have been calculated with full-vector finite difference method (FDM). Figure 3 shows refractive index parameters and position shift of bottom corner of Au layer from top center of the waveguides. In case of InP waveguide, we have used undoped InGaAsP multi-quantum-well structure (MQW) as core material. It consists of 22-pair quantum wells (well – 1.48Q, 10 nm, barrier – 1.15Q, 8 nm) and bottom and top separate-confined-heterostructure (SCH) layers (1.15Q, 100 nm for each layer). It shows photoluminescence (PL) peak wavelength of 1.41~1.42 μm. The design of MQW is suited for Mach-Zehnder electro-optic modulator. The refractive index of SiO_2,

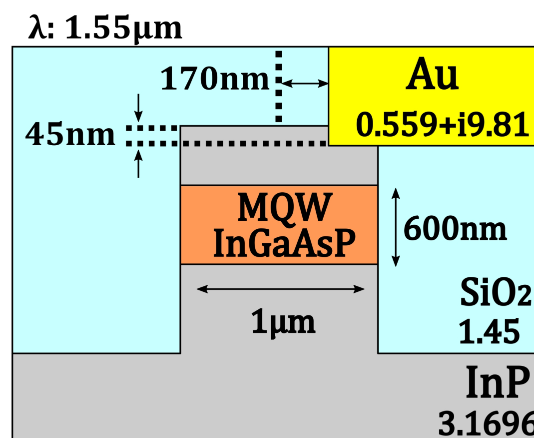

Fig. 3. Simulation condition of InP polarization rotator.

Au, InP, 1.15Q-InGaAsP, and QWs are set as 1.45, 0.559 + i9.81, 3.1696, 3.3038, and 3.3893, respectively, at 1.55 μm. We assumed the refractive index of well and barrier in QWs as effective medium index of 3.3038. The position of the bottom corner of the Au is shifted 170 nm in lateral direction, and 45 nm in vertical direction are shifted with a thickness of 300 nm-InP topcladding. During simulation, we set mesh size as 10 nm for whole region and 2 nm for the bottom corner of the Au layer. Calculated effective indices are 3.2011 + i0.00076 and 3.1903 + i0.00285, with TE power of 49 and 51% for InP waveguide.

2.3 InP polarization rotator

In our study, we have fabricated a deep-ridge waveguide using an InP-InGaAsP multi-quantum-well (MQW) structure. A schematic diagram is shown in Fig. 4. Figure 4(a) shows the whole structure of the device. The waveguide has an S-bend to avoid scattered light coupling between the incoming optical fiber and the output fiber. On the device end sides, the width of the waveguide widens from 1 μm to 6 μm to expand the mode field size to match the optical fiber better. Incident linearly polarized light (TE/TM) goes through the polarization rotator and converts into its orthogonal state (TM/TE). Figure 4(b) shows an isometric view of the polarization rotator. The whole waveguide structure is covered with a SiO_2 dielectric layer of 600-nm thickness. The InP topcladding layer is partially etched to make the deposited 100-nm Au layer of form an orthogonal corner, which controls the rotation degree of the eigenmodes axes in the waveguide. The length of the rotator range is 48 μm. Figure 4(c) shows a cross-sectional view of the rotator. The waveguide width is 1 μm and the thickness of

the InGaAsP MQW core is 600 nm. The thickness of the InP topcladding is 370 nm and the partial etch depth is 200 nm. The corner of the etched position is shifted 100 nm from the center of the waveguide core. Since the SiO_2 layer covers the whole structure except the partially etched region, the deposited Au layer contacts InP only in that section. The 250-nm width of the SiO_2 sidewall is enough to disregard the light coupling between the core and Au sidewalls. Figure 4(d) shows the electric field distribution of the rotated fundamental eigenmodes of the rotator. The electric field of the core interacts with the two orthogonal edges at the left bottom corner of the metal, and is aligned diagonally. However, with only the rotated mode profile of the ridge waveguide, it is unclear whether the rotation angle is exactly 45°, contrary to the channel waveguide. The rotation angle can be quantized by the ratio of the integration of the polarized electric field distribution as follows,

$$\frac{\int |E_x|^2 dxdy}{\int (|E_x|^2 + |E_y|^2) dxdy} \times 100\% \tag{1}$$

When the ratio approaches 50%, the rotation angle becomes 45°. In addition, this ratio is affected by fabrication irregularities such as metal position shift, partial etch depth, and InP topcladding thickness.

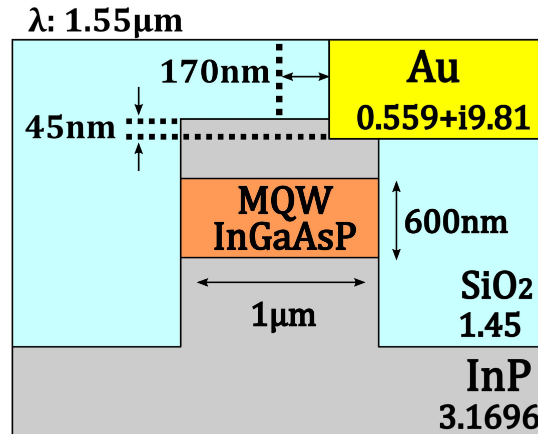

Fig. 4. Schematic diagram of the polarization rotator structure. (a) Whole device structure. Linearly polarized TE/TM modes launched into the device pass through the polarization rotator and their polarity is converted to the orthogonal state (TM/TE). (b) Isometric view of the polarization rotator. (c) Cross-sectional view of the rotator. Corner depth in the topcladding of 370-nm thickness is 200 nm and shifted 100 nm from the waveguide center. (d) Electric field distributions of the rotated fundamental eigenmodes of the rotator.

The effect of these fabrication errors on the power ratio is shown as a contour map in Fig. 5. The inset describes the parameter condition of the X- and Y-axes. The top cladding thickness is set to 375 nm, the partial etch depth is varied from 0 to 280 nm, and the position shift of the metal corner from the waveguide center is varied from 0 to 500 nm. The TE power ratio is shown as ± 10% from 50%. This corresponds to a ± 9° deviation from 45° of the rotation angle. The resulting ± 9° deviation leads to a TE/TM extinction ratio of 9.76 dB. TE power ratio of the green region represents a deviation angle within ± 2.7°, corresponding to the extinction ratio of 20.49 dB. The fabrication tolerance of this region is 240 nm for the partial etch depth and 225 nm for the metal position shift. This tolerance is varied with respect to the topcladding thickness.

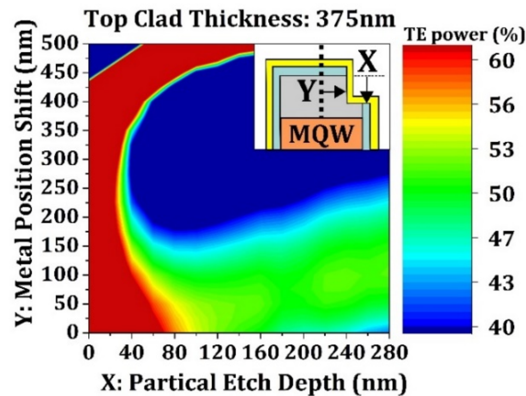

Fig. 5. Contour map of the TE power ratio with respect to a topcladding thickness of 375 nm, partial etch depth along the X-axis, and metal position shift of the Y-axis. The inset indicates XY-axes parameters with respect to the topcladding layer etching condition. The contour map distribution describes the fabrication error tolerance. A TE power of 50% means an ideal 45° rotation of the eigenmode axes. The green region represents the deviation angle within ± 3°, corresponding to the extinction ratio of 20.49 dB with a fabrication tolerance of more than 200 nm in toplcadding etching conditions.

Figure 6 shows the three-dimensional transmission simulation results at 1.55 μm using the eigenmode expansion (EME) method. The simulation condition is same as that of the structure shown in Fig. 3. Figure 6(a) shows the transmittance results with respect to the rotator length. The blue line indicates the calculated TE power after passing through the polarization rotator and the red dashed line is for the calculated TM power. The TE power drops as the rotator length increases. It reaches the minimum at a rotator length of approximately 47 μm of. The TM power rises as the rotator length increases. It reaches the maximum at approximately 40 μm. The discrepancy in the rotator length between the maximum and minimum points is due to the absorption loss of the metal. The total loss of the device with the length of 47 μm is approximately −2.5 dB.

When comparing with the previous plasmonic polarization rotator results, this device loss is low because the metal and core are apart and only the partial portion of the metal interacts with light. It can be further reduced by lowering the partial etch depth. Figure 6(b) shows the simulation result for the intensity of light at the device length of 47 μm and disappearing electric field intensity profile when launching the TE (Ex) mode into the polarization rotator marked as a dotted line. The disappearing TE mode is converted to the TM (Ey) mode as shown in the Fig. 6(c).

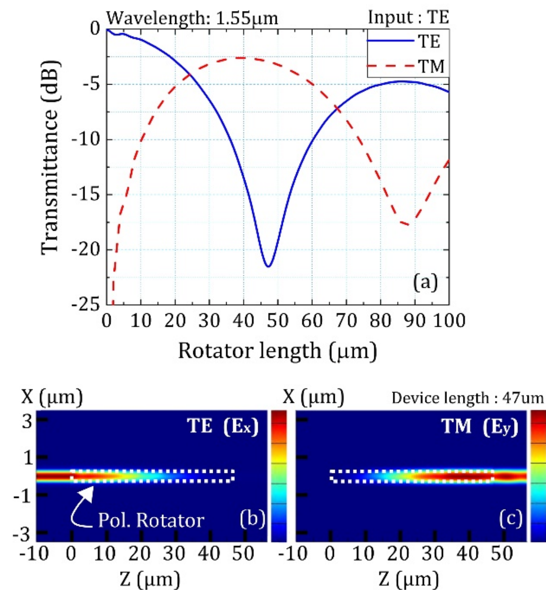

Fig. 6. Three-dimensional simulation results of the transmission characteristics of the polarization rotator. Figure 6(a) shows the transmitted optical power (TE–blue, TM–red dashed lines) when launching the TE mode into the device. The maximum conversion and extinction ratio efficiency is obtained at a device length of 47 μm of the device length. The converted TM power has a −2.5 dB loss due to metal absorption loss. The electric field intensity distribution of the TE (Ex) mode and TM (Ey) mode are shown in Figs. 6(b) and 6(c), respectively.

3. Fabrication process

Fabrication process of the polarization rotator is shown in Fig. 7. (a) First, undoped InP layer of 370 nm thickness is grown by metalorganic chemical vapor deposition (MOCVD) on MQW layer. The thickness of the top InP layer is precisely controlled by epitaxial growth. (b) SiO_2 layer of 300 nm thickness is deposited by plasma enhanced chemical vapor deposition (PECVD). Then, positive photoresist (AZ 5214) is spin-coated and baked at 100°C for 1 min. After that, waveguide pattern is defined in the photoresist via photolithography and development processes. Waveguide pattern is transferred to SiO_2 layer by dielectric reactive ion etching (RIE) process. Remaining photoresist layer is removed by wet chemical etching and microwave ashing process. Pattern in SiO_2 layer is transferred to InP wafer by inductively coupled plasma (ICP) etching. Total etching depth is about 3 μm. (c) SiO_2 hard mask is

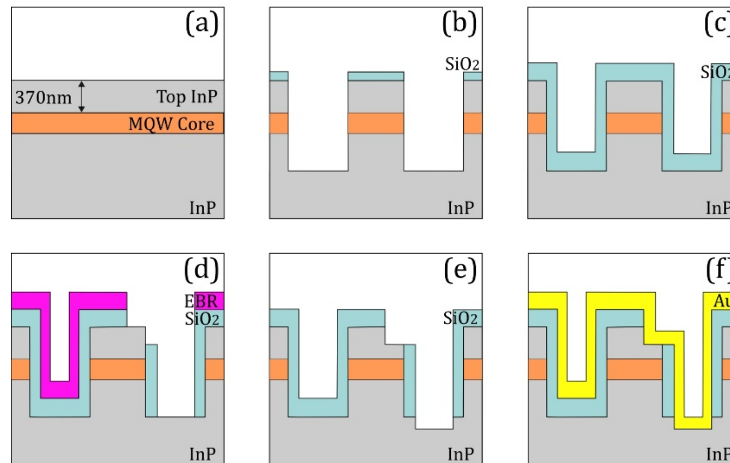

Fig. 7. Fabrication process of InP polarization rotator.

removed and new SiO_2 layer of 600 nm thickness is deposited by tetraethyl orthosilicate (TEOS) PECVD. Here, TEOS source is used for high step coverage because it ensures wider SiO_2 sidewall, which separates InP waveguide sidewalls and deposited Au layer. In addition, TEOS PECVD process is carried out at 250°C to prevent unwanted diffusion effect in InP wafer. (d) Electron-beam resist (ZEP520A) is coated to pattern SiO_2 layer. We have used electron-beam lithography instead of photolithography for precise placement of the partial etch region. ZEP520A is coated twice with 1200 rpm and baked at 180°C for 2 min at each spin-coating process. The coated thickness at top InP cladding is more than 1 μm. ZEP520A is patterned by 100 keV electron beam lithography system (nB4 from Nanobeam ltd.) and developed. Developed area is shifted 100 nm from the center of the waveguide. Developed resist pattern is transferred to SiO_2 layer by RIE process. Etching depth is more than 600 nm for complete removing of SiO_2 layer at InP topcladding. (e) Remaining resist is removed by microwave ashing process. Opened InP topcladding area is etched by 200 nm in depth. (f) Finally, Au layer of 200 nm thickness is deposited by RF magnetron sputtering. InP wafer is cleaved and fabrication process is finished.

Figure 8 shows a cross-sectional scanning electron microscope (SEM) image of the polarization rotator. The topcladding is partially etched to a depth of 190 nm in depth and the bottom corner is shifted 100 nm from the waveguide center. The deposited Au covers the partially etched region. It shows a trapezoidal waveguide structure due to the unoptimized fabrication process. The width of the MQW core at the midpoint is approximately 870 nm, which has a 130 nm difference from the rotator design with a rectangular shape. However, its performance is excellent, and it proves the fabrication tolerance of the device.

4. Characterization of InP polarization rotator

Figure 9 shows the schematic of the characterization setup used in the main text. We have used an external-cavity laser (ECL, Keysight 81989A) for optical C-band wavelength sweep. Launched TM mode light from ECL source is converted to TE mode via a three paddle polarization controller. A Polarization beam splitter (PBS, from OZ optics) filters TM mode, which increases TE/TM extinction ratio of the light source. Filtered light source through singlemode fiber (SMF) is converted into light propagating in the free space using fiberport collimators (FC, from Thorlabs) and vice versa. A quarter-wave plate (λ/4) is used to compensate for any unwanted circular polarization introduced by the optical fiber and a half-wave plate (λ/2) is used to compensate for rotate angle errors of the TE output light. Light is

Optics EXPRESS

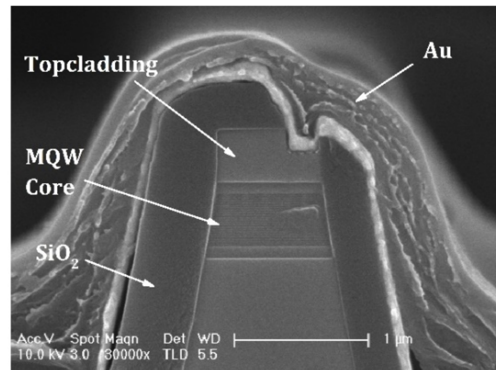

Fig. 8. SEM image of the fabricated InP polarization rotator.

coupled into polarization maintaining lensed fiber (lensed PMF, from LovaLite). The axes of PMF is adjusted with a fiber rotator (FR). TE mode light is launched into the InP polarization rotator chip and converted into TM mode. The output TM mode light is coupled into lensed PMF. Quarter-wave and half-wave plates are used again to compensate for circular polarization and rotation angle. A polarizer is used to distinguish TE/TM power ratio. Filtered light power is measured with optical power meter (OPM, Keysight 81635A).

Figure 10 shows measured transmission spectrum results. Figure 10(a) shows transmission spectrum of a reference InP waveguide without the polarization rotator. In Fig. 10(a), red dotted and black solid lines show measured TE and TM modes, respectively. Spectral response of the measurement setup shows a resonance condition for both TM/TE results at the same wavelength as peak/valley with free spectral range (FSR) of 5.6 nm. Figure 10(b) shows transmission spectrum of the polarization rotator with a length of 48 µm. It also shows the resonance condition with FSR of 5.6 nm. In case of the polarization rotator, the extinction ratio between TM/TE powers is more than 20 dB.

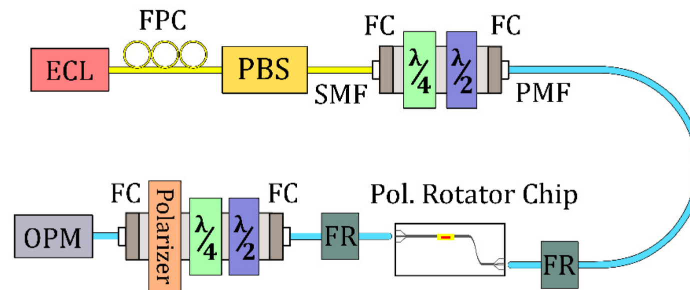

Fig. 9. Schematic of the characterization setup. ECL: external cavity laser. PBS: polarization beam splitter. λ/4, λ/2: rotating wave plates. FR: fiber rotator, OPM: optical power meter.

Polarization state of the measurement setup is wavelength dependent by wave plates for polarization control and also affected by internal reflection/misalignment in fiber to fiber coupling. Previous results have spectral ripples for the internal polarization rotation, which disturbs exact measurement of the extinction ratio [12] [22]. Our result looks similar to Zhang's result [20] using plasmonic effect based on mode evolution method. It shows high extinction ratio over the whole spectral range. Contrary to [20], our device uses plasmonic effect based on half-wave retardation. Therefore, TM/TE output reaches equal with same FSR as wavelength sweeps due to the internal polarization rotation of the measurement setup. TM/TE power difference at the resonance wavelengths means the extinction ratio.

Figure 10(c) shows the extinction ratio comparision spectrum between the reference waveguide and the polarization rotator length of 48 μm. In Fig. 10(c), the polarization state of the measurement system was controlled for each wavelength measurement. The reference TE power is shown as red solid line and the rotated TM power is shown as a black dashed line. The power difference of about 2.5 dB is the rotator device loss. The extinction ratio between TM/TE powers of the rotator is more than 20 dB over the whole C-band (1530–1565 nm). Figure 10(d) shows a comparison of the extinction ratio between simulation result and measured values.

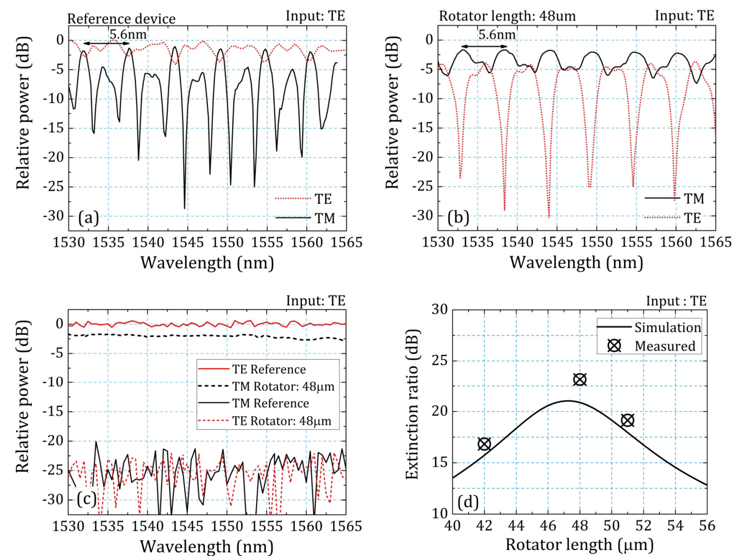

Fig. 10. Transmission spectrum of the polarization rotator.

5. Conclusions

We have proposed an InP integrated polarization rotation scheme using the plasmonic effect as half-wave retardation. We have shown that a strong surface plasmon effect at the orthogonal metal corner can control the state of the polarization in the neighboring waveguide precisely. This strong yet indirect method can be applied to any dielectric material system and waveguide type. This is the distinguished novelty of the proposed method over the previous plasmonic rotators that use the plasmonic effect as a mode evolution method. By utilizing this phenomenon, an epitaxially grown InP- InGaAsP MQW deep-ridge waveguide can work as a polarization rotator. The eigenmode axes of the MQW waveguide are aligned diagonally to work as a half-wave retarder. The fabricated device exhibited an extinction ratio of more than 20 dB over the C-band. The measured device loss is approximately −2.5 dB, which is relatively high comparing to previous results. We believe that the proposed method can be applied to further complex PDM technology to boost the spectral efficiency [26].

Funding

'The Cross-Ministry Giga Korea Project' grant from the Ministry of Science, ICT and Future Planning, Korea.

129.254.34.16 {ts '2018-01-17 21:27:05'}